https://doi.org/10.26866/jees.2025.1.r.277 ISSN 2671-7263 (Online) · ISSN 2671-7255 (Print)

Super-Resolution Angle Estimation Algorithm using Low Complexity MUSIC-Based RELAX for MIMO FMCW Radar

Bong-Seok Kim¹ 📵 · Youngseok Jin¹ 📵 · Jonghun Lee² 📵 · Sangdong Kim²,* 📵 · Ram M. Narayanan³,* 📵

Abstract

A novel super-resolution angle estimation algorithm using low complexity-multiple signal classification (LC-MUSIC)-based relaxation (RELAX) for multiple-input multiple-output (MIMO) frequency-modulated continuous-wave (FMCW) radar is proposed in this paper. FMCW radar is widely used to estimate target location information in various fields, including autonomous driving, defense, and robotics. However, FMCW radar struggles to provide high-resolution direction of arrival (DOA) data. To obtain precise target positions, especially for multiple targets, FMCW radar with high-resolution DOA capability is needed. Conventional FMCW radar employs MIMO-based technology to improve angular resolution because of its low complexity and ease of implementation, but MIMO-based radar still struggles to provide precise angular resolution. To improve the angle resolution, we propose a novel super-resolution DOA algorithm in a MIMO scheme. The new method consists of RELAX-based CLEAN and LC-MUSIC. Combining the MIMO technique with the new super-resolution algorithm enables FMCW radar with high angular resolution to be obtained. To analyze the performance of the proposed estimation, Monte Carlo simulations are performed, and root-mean-square error results are analyzed. Using the FMCW radar module, experiments comparing the proposed and conventional algorithms were performed in an indoor environment.

Key Words: Direction of Arrival, FMCW Radar, MIMO, RELAX, Super-Resolution.

I. Introduction

Radar systems are widely utilized to precisely detect, track, and classify targets in airborne, surveillance, and autonomous vehicle applications. These radar sensors operate well in various weather conditions and both day and night, unlike, for example, camera and LIDAR sensors. In the past, mechanical scanning of antennas has been used to obtain radar results. Synthetic aperture radar is used as a replacement for high-resolution radar using a moving antenna platform. Autonomous driving applica-

tions use a large number of transmit and receive elements-based frequency-modulated continuous-wave (FMCW) phased-array radar systems [1–3]. Detecting the angles where humans are located is a particularly important issue in finding a precise position for FMCW phased-array radar [4, 5]. Digital beamforming has generally been utilized through the fast Fourier transform (FFT) algorithm to obtain direction of arrival (DOA) results. However, the DOA parameter estimator based on FFT has notably low resolution and accuracy [4].

Better radar performance can be achieved by utilizing a mul-

Manuscript received January 08, 2024; Revised May 29, 2024; Accepted June 11, 2024. (ID No. 20240108-008J)

This is an Open-Access article distributed under the terms of the Creative Commons Attribution Non-Commercial License (http://creativecommons.org/licenses/by-nc/4.0) which permits unrestricted non-commercial use, distribution, and reproduction in any medium, provided the original work is properly cited.

¹Division of Automotive Technology, Daegu Gyeongbuk Institute of Science and Technology (DGIST), Daegu, Korea.

²Division of Automotive Technology and the Department of Interdisciplinary Engineering, DGIST, Daegu, Korea.

³Department of Electrical Engineering, Pennsylvania State University, University Park, PA, USA.

^{*}Corresponding Author: Sangdong Kim (e-mail: kimsd728@dgist.ac.kr), Ram M. Narayanan (e-mail: rmn12@psu.edu)

[©] Copyright The Korean Institute of Electromagnetic Engineering and Science.

tiple-input multiple-output (MIMO) FMCW architecture [6], which has the advantage of having a smaller antenna than phased-array radar. The MIMO-based FMCW radar system can be established using the time division multiplexing (TDM) method to switch between transmit antenna elements. The switching method using TDM achieves the final number of virtual antennas given by the product of the transmit and receive elements. For indoor applications, a portable platform-installed small radar system is urgently needed. Several studies of MIMO radar have been proposed [7–9]. For short-range applications, the MIMO radar system can provide high-resolution angular results. However, to achieve precise location information, this solution requires further improvement in angular resolution.

To improve the angular resolution, we propose a new super-resolution algorithm for a MIMO scheme. This method consists of a relaxation (RELAX)-based CLEAN and multiple signal classification (MUSIC) algorithms. Combining the MIMO technique with the new super-resolution algorithm, called low-complexity MUSIC-based RELAX (LC-MELAX), enables the implementation of high-resolution FMCW radar. The LC-MELAX algorithm has high complexity because it uses low-complexity MUSIC (LC-MUSIC) repeatedly. The LC-MELAX is required to solve this problem. The basis of the proposed system is that the wide bandwidth of the FMCW radar has high range resolution while the MIMO-based ME-LAX algorithm has high angular resolution. The system architecture of the radar system is presented in the next section with an in-depth description.

This paper is structured as follows. For the range and angle of the MIMO-based FMCW radar, Section II presents the basic principles of the system model. Section III provides the proposed MELAX algorithm-based MIMO technique for FMCW radar. Sections IV and V present the simulation and experimental results for various parameters, respectively. Finally, conclusions are provided in Section VI.

II. SYSTEM MODEL

This section presents the system model for the MIMO-based FMCW radar. We consider MIMO TDM FMCW radar systems with P transmit (TX) antennas and Q receive (RX) antennas [10] in this paper. Fig. 1 illustrates the TX signal of a typical MIMO-based FMCW radar system with a saw-tooth waveform where T_c is the time duration of a chirp signal, and f_0 and B are the center frequency and bandwidth of the system, respectively. The TX FMCW signal x(t) is given by:

$$x(t) = \begin{cases} \exp\left(j2\pi\left(f_0t + \frac{\mu}{2}t^2\right)\right) & \text{for } 0 \le t \le T_c, \\ 0 & \text{elsewhere} \end{cases}$$
 (1)

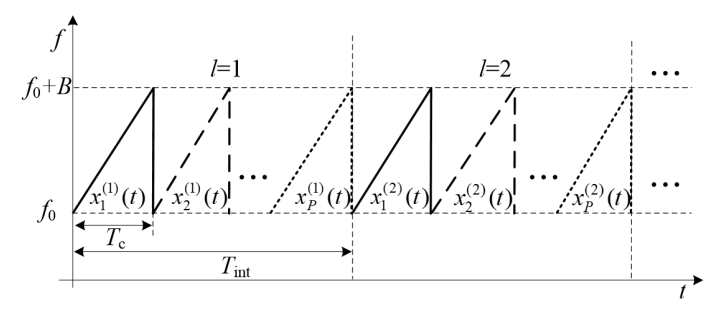


Fig. 1. Signal of typical TDM MIMO-based FMCW radar.

where $\mu = B/T_c$ is the frequency rate of the FMCW signal, and l is the frame index. The TX signal x(t) generates the continuous wave signal, which is emitted to a target through a TX antenna with time duration T_{int} . The TX FMCW radar signal from the p-th TX antenna at the l-th frame for $1 \le p \le P$ and $1 \le l \le L$ is denoted as $x_n^{(l)}(t)$ and is given by:

$$x_n^{(l)}(t) = x(t - (p - 1)T_c - (l - 1)T_{\text{int}}). \tag{2}$$

Fig. 2 illustrates the antenna structure of a typical MIMO-based FMCW radar system. The TX part is at the l-th frame, and the RX part is at the p-th TX signal, as shown in Fig. 2(a) and 2(b), respectively. d_T and d_R are the distances between adjacent TX antennas and RX antennas, respectively, in Fig. 2. As in Fig. 2(a), the FMCW TX signal $x_p^{(l)}(t)$ transmits sequentially through the P TX antennas. Then, $x_p^{(l)}(t)$ is re-

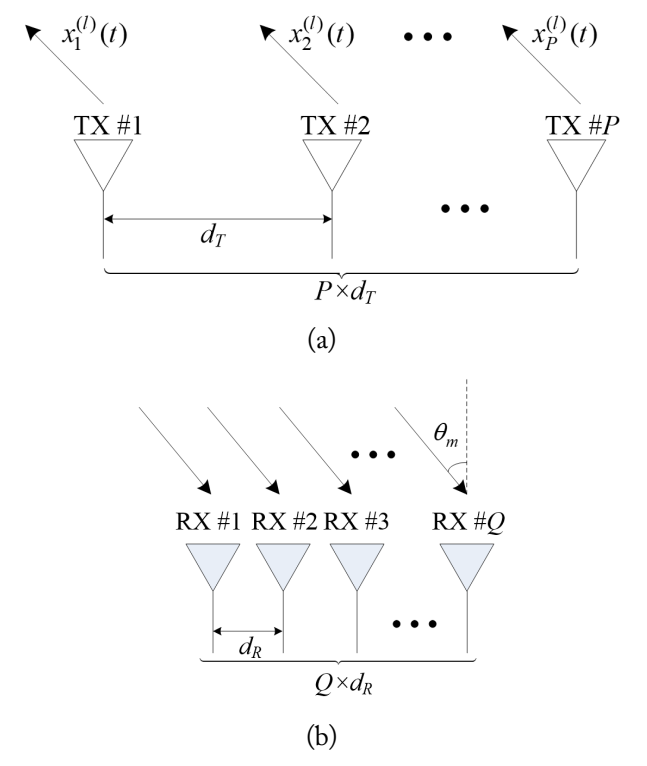


Fig. 2. Antenna structure of typical MIMO-based FMCW radar: (a) TX part at the *l*-th frame and (b) RX part at the *p*-th TX signal.

flected by the M targets and is received by a total of Q RX antennas, as in Fig. 2(b).

An analog-to-digital converter (ADC) is used to convert the analog RX signals into digital signals with sampling frequency f_s . The sampled RX signal is transmitted from the p-th TX antenna and received by the q-th RX antenna and is denoted by $y_{p,q}[n,l]$. The primary goal of MIMO-based FMCW radar is to estimate the parameters for range and angle information, except Doppler information. The Doppler information is omitted by employing only one chirp symbol, namely, $y_{p,q}[n,l]$, which can be simply expressed as $y_{p,q}[n]$ by omitting the frame index l. The sampled beat signal $y_{p,q}[n]$ is expressed as:

$$y_{p,q}[n] = \sum_{m=1}^{M} a_m \exp \left(j2\pi \left(\underbrace{\frac{\mu \tau_m n}{f_s}}_{\text{range term}} + \underbrace{\frac{d_{p,q} \sin(\theta_m)}{\lambda}}_{\text{angle term}} \right) \right) + z_{p,q}[n], \text{ for } 0 \le n \le N_s - 1,$$
(3)

where N_s is the number of samples, a_m represents the complex amplitude, τ_m is the delay in which the distance between the m-th target and the radar is converted, θ_m is the DOA of the m-th target, $d_{p,q}$ is the relative distance made by the p-th TX and antenna and the q-th RX antenna, that is, $d_{p,q} = d_T(p-1) + d_R(q-1)$, λ is the wavelength, and $z_{p,q}[n]$ is the additive white Gaussian noise. The amplitude a_m with complex value consists of the amplitude term \tilde{a}_m due to the reflected effect at the m-th target and the Doppler effect due to the TX timing difference, that is, $a_m = \tilde{a}_m \exp(j2\pi f_{D,m}(p-1)T_c)$, where $f_{D,m}$ represents the m-th target-based Doppler frequency.

III. PROPOSED MELAX ALGORITHM FOR MIMO FMCW RADAR

For the MIMO FMCW radar, the proposed novel algorithm based on super-resolution is described in this section. Fig. 3 represents the proposed algorithm. As shown in Fig. 3, first, range estimation based on the N_R -point FFT is achieved on the ADC beat signal $y_{p,q}[n]$, and the r-th FFT output $Y_{p,q}[r]$ is obtained, as follows:

$$Y_{p,q}[r] = \sum_{N_S-1}^{N_S-1} y_{p,q}[n] \exp(-j2\pi nr/N_R), \text{ for } 0 \le r \le N_R - 1.$$
 (4)

Then, peak detection of FFT outputs is performed to select range bins where targets are estimated to exist. This reduces unnecessary computations in the angle estimation process, as

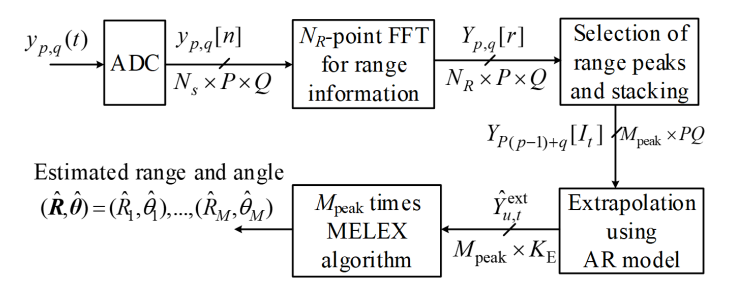


Fig. 3. Structure of the proposed algorithm.

empty range bins are not considered. We denote the number of total peaks among the range bins as M_{peak} , and the index vector of peaks I is selected, that is, $I = [I_1, I_2, ..., I_{M_{peak}}]$. The index vector of peaks I refers to the information in range bins where targets exist among all range bins. After the selection of the peak indices, the data for the P TX and Q RX antennas are stacked. That is, the I_t -th stacked angular vector is denoted by $Y[I_t]$ for $1 \le t \le M_{peak}$, and it is expressed as:

$$\boldsymbol{Y}_{t} = \left[Y_{1}[I_{t}], Y_{2}[I_{t}], \dots, Y_{P(p-1)+q}[I_{t}], \dots Y_{PQ}[I_{t}] \right]^{T}.$$
 (5)

This 2D stacked data matrix Y with $PQ \times M_{peak}$ is represented as follows:

$$\mathbf{Y} = \begin{bmatrix} Y_{1} & Y_{2} & \cdots & Y_{M_{\text{peak}}} \end{bmatrix} = \begin{bmatrix} Y_{1}[I_{1}] & Y_{1}[I_{2}] & \cdots & Y_{1}[I_{M_{\text{peak}}}] \\ Y_{2}[I_{1}] & Y_{2}[I_{2}] & \cdots & Y_{2}[I_{M_{\text{peak}}}] \\ \vdots & \vdots & \ddots & \vdots \\ Y_{PQ}[I_{1}] & Y_{PQ}[I_{2}] & \cdots & Y_{PQ}[I_{M_{\text{peak}}}] \end{bmatrix}$$
(6)

The stacked data matrix Y is used as the input to the extrapolation algorithm, called an autoregressive (AR) model [11], for pre-processing to improve resolution before the LC-MELAX operation. The u-th extrapolated data at the t-th peak $\hat{Y}_u^{ext}[I_t]$ is obtained as follows:

$$\hat{Y}_{u}^{\text{ext}}[I_{t}] = -\sum_{k=1}^{N_{p}} \alpha_{k} Y_{u-k}[I_{t}] \text{ for } N_{P} + 1 \le u \le K_{E},$$
(7)

where N_p is the model order, α_k values are the AR components, and K_E is the number of extrapolated data samples. The extrapolated data $\hat{Y}_u^{ext}[I_t]$ are expressed in vector form \boldsymbol{Y}_t^{ext} , that is, $\boldsymbol{Y}_t^{ext} = [\hat{Y}_1^{ext}[I_t], \hat{Y}_2^{ext}[I_t], ..., \hat{Y}_{K_E}^{ext}[I_t]]$, and employed as input to the proposed super-resolution algorithm, which is called the LC-MELAX algorithm, as shown in Fig. 4.

The LC-MELAX algorithm is a combination of the RE-LAX and LC-MUSIC algorithms. The RELAX algorithm is a kind of CLEAN algorithm that is used to estimate frequency with high resolution [12]. As shown in Fig. 4, the RELAX algo-

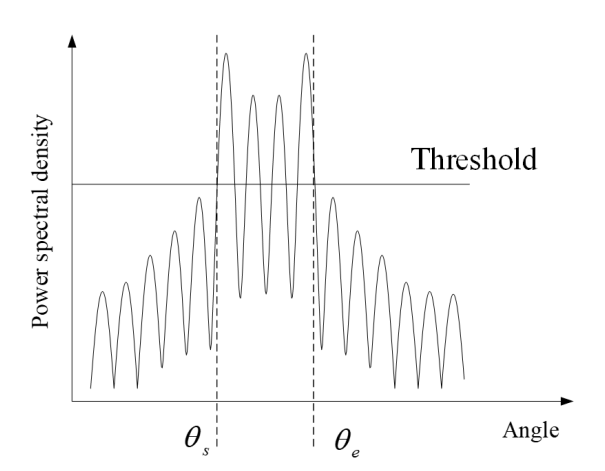


Fig. 4. Start of target angle θ_s and end of target angle θ_e .

rithm first performs FFT on the input signal and then estimates the frequencies corresponding to the peaks of the magnitude of the FFT output. The complex sinusoidal signals of the estimated frequencies are generated. After the generated sinusoid signal is subtracted from the input signal, the FFT is performed on the remaining signal. By repeating this process, high-resolution frequencies are estimated.

The LC-MELAX algorithm uses LC-MUSIC instead of FFT. As the first step of the LC-MELAX algorithm, the LC-MUSIC algorithm is performed. The extrapolated signal \boldsymbol{Y}_t^{ext} obtains the angle spectrum results through FFT as follows:

$$Y_{FFT}^{ext} = DY_t^{ext}, (8)$$

where ${\bf D}$ is $N \times K_E$ matrix for an FFT operation. The FFT consists of column vectors such as ${\bf D} = \left[{\bf D}_0, {\bf D}_1, {\bf D}_2, ..., {\bf D}_{K_E-1} \right]$ where ${\bf D}_k = \left[1, \exp\left(- \frac{j2\pi k}{N} \right), \exp\left(- \frac{j4\pi k}{N} \right), ..., \exp\left(- \frac{j2\pi (N-1)}{N} \right) \right]$. This FFT spectrum results can detect the start of target angle θ_s and the end of target angle θ_e through the target threshold detection. θ_s and θ_e are expressed in Fig. 4.

Then, the extrapolated signal $\hat{Y}_u^{ext}[I_t]$ is used as the input of the correlation matrix R_t , calculated as:

$$\mathbf{R}_t = \mathbf{Y}_t^{ext} (\mathbf{Y}_t^{ext})^H, \tag{9}$$

where $(\cdot)^H$ is the Hermitian operator. The forward-backward technique achieves the correlation smoothing effect, such that:

$$\boldsymbol{R}_{t}^{fb} = \frac{1}{2} (\boldsymbol{R}_{t} + \boldsymbol{J} \boldsymbol{R}_{t}^{*} \boldsymbol{J}), \tag{10}$$

where J is the size of the $K_E \times K_E$ -based exchange matrix. Eigenvalue decomposition (EVD) [13, 14] is used to process the autocorrelation matrix \mathbf{R}_t^{fb} as:

$$\mathbf{R}_{t}^{fb} = \begin{bmatrix} \mathbf{S} & \mathbf{N} \end{bmatrix} \begin{bmatrix} \sigma_{1} & 0 & \vdots & 0 \\ 0 & \sigma_{2} & \ddots & \vdots \\ \vdots & \ddots & \ddots & 0 \\ 0 & \cdots & 0 & \sigma_{K_{\mathbf{P}}} \end{bmatrix} \begin{bmatrix} \mathbf{S}^{*} \\ \mathbf{N}^{*} \end{bmatrix}$$
(11)

where the eigenvectors are composed of the signal eigenvector matrix $S = [s_1, ..., s_M]$ and the noise eigenvector matrix $N = [n_1, ..., n_{K_E-M}]$. The signal eigenvector matrix S with the dimension M and the noise eigenvector matrix N with dimension $K_E - M$ span the signal subspace and the noise subspace, respectively. Furthermore, σ_n represents the n-th eigenvalues of the autocorrelation matrix R_t^{fb} . The largest M eigenvalues of $\sigma_1, ..., \sigma_M$ correspond to the M signal eigenvectors of S. The remaining eigenvalues $\sigma_{M+1}, ..., \sigma_{K_E}$ correspond to the noise eigenvectors of N, that is, $\sigma_{M+1} = \cdots = \sigma_{K_E} = \varepsilon^2$. The decreasing order-based eigenvalue is expressed as:

$$\sigma_1 \ge \sigma_2 \ge \dots \ge \sigma_M \ge \sigma_{M+1} = \dots = \sigma_{K_F} = \varepsilon^2.$$
 (12)

The results of the LC-MUSIC algorithm use the orthogonality of the target-based steering angular vector $\psi(\theta)$ and the noise subspace N, that is:

$$\psi(\theta)\mathbf{N}^H = 0, \tag{13}$$

where $\psi(\theta)$ is defined as:

$$\psi(\theta) = \begin{bmatrix} 1, \exp\left(j2\pi\left(\frac{d_R}{\lambda}\right)\sin(\theta)\right), \\ \dots, \exp\left(j2\pi\left(\frac{d_R(K_E - 1)}{\lambda}\right)\sin(\theta)\right) \end{bmatrix}$$
(14)

where the range of θ consists of θ_s and θ_e . Through the property of (13), in the first target among M humans, the angular LC-MUSIC spectrum $P_{\text{MUSIC}}(\theta)$ can be obtained from:

$$P_{\text{MUSIC}}(\theta) = \frac{1}{\psi(\theta) N^H N \psi^H(\theta)}.$$
 (15)

After the first LC-MUSIC step, the angular components of the angle value are obtained using threshold detection. Based on the estimated angular components, maximum peak detection is performed. Then, the generated sinusoidal signal is subtracted from the original angular signal. The subtracted original angular signal is fed into the input of the second LC-MUSIC step. The second LC-MUSIC step is processed as in (9) and repeated until the peak no longer exists. Because the result of the LC-MUSIC algorithm provides a significant improvement in resolution performance compared to FFT, the LC-MELAX algorithm is expected to achieve an even greater improvement in performance than the RELAX algorithm.

The principal steps of the proposed algorithm are as follows:

- Step 1: To obtain range estimation, the received chirp signals with the first chirp index; the *p*-th TX and the *q*-th RX antenna array become the input of the range FFT.
- Step 2: After the range FFT produces the target's range information, we extract the angular information through the

magnitude and phase information of the detected range FFT results.

- Step 3: To precisely obtain angles, we accomplish the extrapolation algorithm using the AR model.
- Step 4: Using extrapolated angular data, we employ the results of the novel MELAX algorithm. Using MELAX, the proposed structure yields high-resolution angular information.
- Step 5: The MELAX process first generates a sinusoidal signal based on the highest magnitude value through MUSIC. Then, the generated sinusoidal signal is subtracted from the original signal. This process is repeated until the peak no longer exists.
- Step 6: Finally, high-resolution range and angular information is obtained, and the high-resolution FMCW radar results are achieved.

All the above steps are shown in Figs. 4 and 5.

IV. SIMULATIONS

The estimation performance of the proposed FMCW radar is verified in this section. Various simulation results indicate that the proposed structure outperforms the conventional structure.

1. Simulation Environment

This paper considers two simulations to validate the angle estimation performance of the proposed structure. In the first simulation, the angle information is obtained by performing the spectrum results of the MELAX-based proposed algorithm and FFT

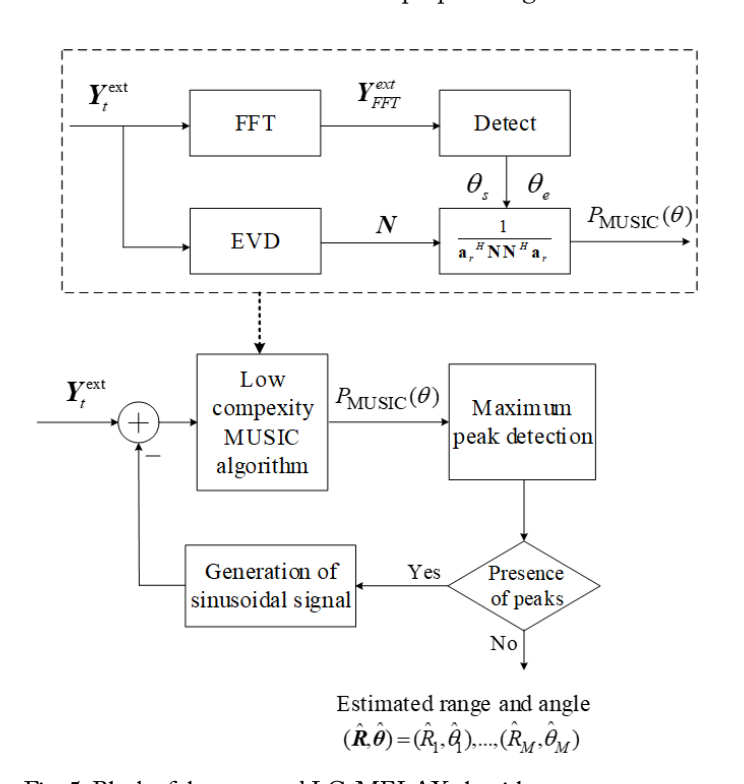


Fig. 5. Block of the proposed LC-MELAX algorithm.

and MUSIC-based conventional algorithms. In the second simulation, we calculate the root-mean-square error (RMSE) of two targets with different angles and the same range. Table 1 lists the simulation parameters of the MIMO-based FMCW radar.

The two targets were placed at a range of 15 m from the radar. Based on a variety of signal-to-noise ratios (SNRs), the angle RMSEs of various algorithms were performed C times, where C means the number of simulations. The average RMSE is represented by $\sqrt{1/C\sum_{n=1}^{C}(\hat{\theta}_n-\theta)^2}$, where the number of simulations C is configured to 10^3 , and $\hat{\theta}_n$ is the estimated angle of the target based on the n-th Monte-Carlo trial.

2. Simulation Results

In this simulation environment, the targets are placed at a range of 15 m from the radar, as shown in Fig. 6. In terms of angle, the proposed algorithm can separate two targets while the conventional algorithms cannot. With $d_T = Q \times d_R$ and $d_R = \lambda/2$, the field-of-view ranges from -60° to 60° [15], and the angular resolution is approximately 9° [16]. The SNR value is set to 20 dB. Fig. 6 shows the simulation environment of the two targets, where S represents the difference distance between the targets and is set

Table 1. Simulation parameters for MIMO-based FMCW radar

Parameter	Value
Bandwidth (GHz)	1.79
Center frequency (GHz)	77
Chirp duration, $T(\mu s)$	60
Number of chirps, L	64
Transmitted channel, P	3
Received channel, Q	4
Number of samples per chirp, N	256

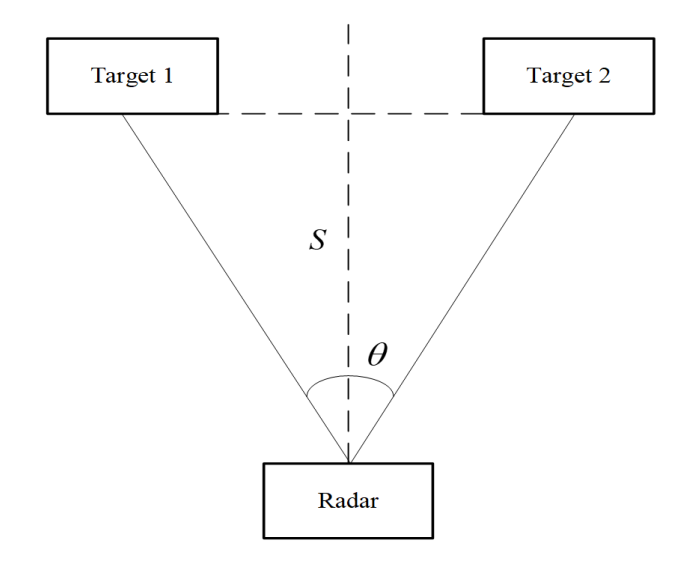


Fig. 6. Simulation environment of the two targets.

to 15 m to evaluate the angle resolution of each algorithm.

In Fig. 7, the spectrum result for each algorithm is obtained using a virtual MIMO array of PQ=12. In Fig. 7(a), the simulation results of the FFT and the RELAX with PQ=12 exhibit two peaks in terms of angle parameter compared to the actual reference signal. All the algorithms can classify the two targets properly when the two objectives are positioned at $\theta_1=20^\circ$ and $\theta_2=38^\circ$, with an angle difference of 18°, as shown in Fig. 6(a). When the two objectives are in close proximity at $\theta_1=20^\circ$ and $\theta_2=29^\circ$, with an angle difference of 9°, all the algorithms can still classify the two targets appropriately, as shown in Fig. 7(b), which is close to the theoretical resolution value.

When the two targets are located very close together at $\theta_1 = 20^\circ$ and $\theta_2 = 24^\circ$ at an angle difference of 4°, the spectrum of the proposed algorithm and RELAX obtain two peaks, while the conventional algorithms cannot separate the two targets, as shown in Fig. 7(c). The proposed algorithm demonstrates the best performance in terms of accuracy. In Fig. 7(d) with $\theta_1 = 20^\circ$ and $\theta_2 = 22^\circ$, at an angle difference of 2°, the proposed

algorithm performs best in terms of accuracy, while the conventional algorithms obtain one peak compared to the actual reference data. Based on these simulation results, the proposed method is suitable for high-resolution FMCW.

Next, the RMSEs of the proposed and conventional algorithms were obtained based on various angle differences for several SNRs with a virtual MIMO array of PQ = 12. This simulation considers the RMSEs of the first target when a second target exists. The angle separations were configured to 18° , 9° , 4° , and 2° , respectively.

With an angle difference of 18°, the RMSEs of all the algorithms, as shown in Fig. 8(a), showed similar performances because the angle difference was sufficiently wide. The proposed algorithm showed higher accuracy than the conventional algorithms. As shown in Fig. 8(b), when the angle difference of two targets approached the resolution limitation with an angle difference of 9°, the proposed structure also achieved the highest accuracy with a virtual MIMO array of PQ = 12 under -8 dB < SNR. When -8 dB \geq SNR, the proposed and conventional

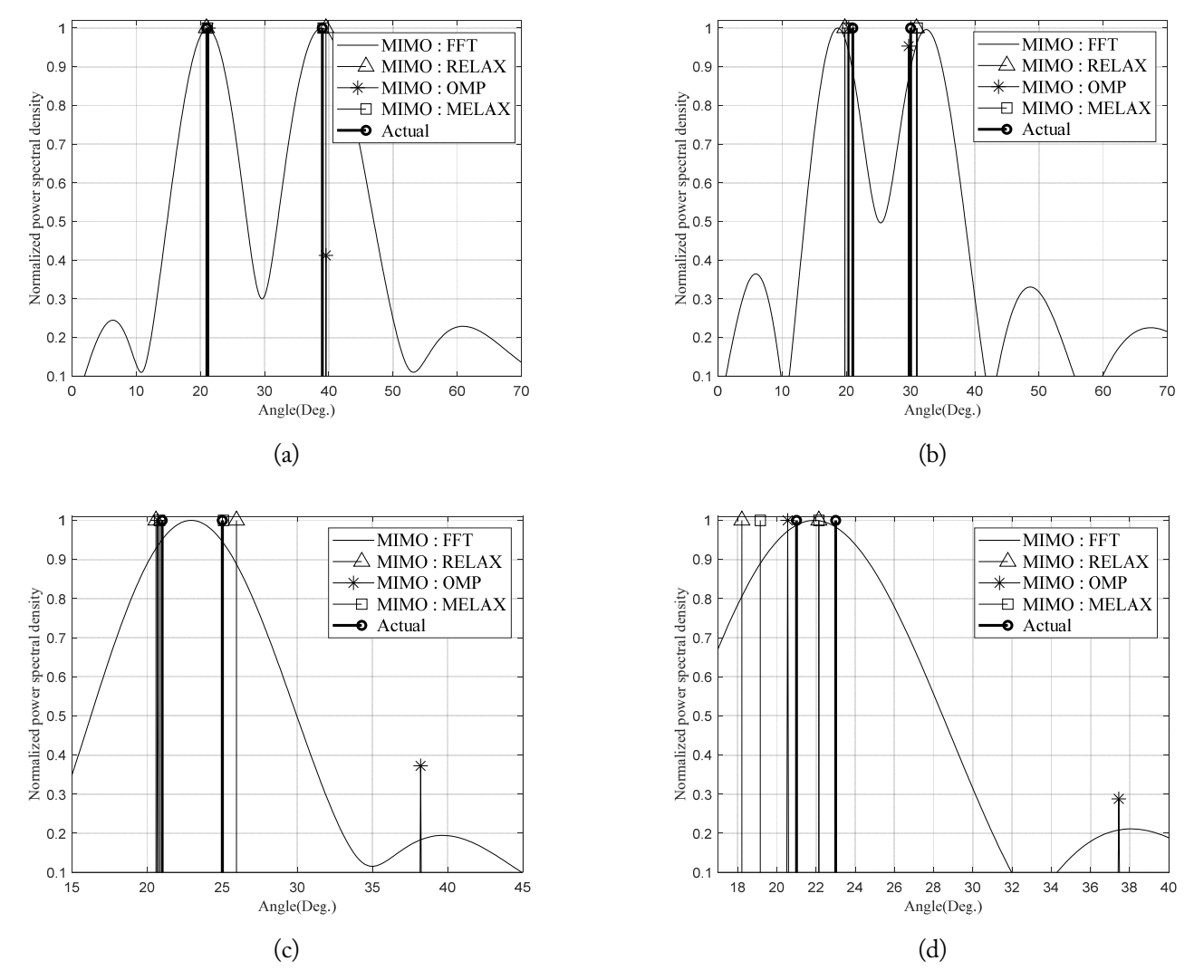


Fig. 7. Simulation environment of the two targets. Spectrum results of angle difference of two targets: (a) 18°, (b) 9°, (c) 4°, and (d) 2°.

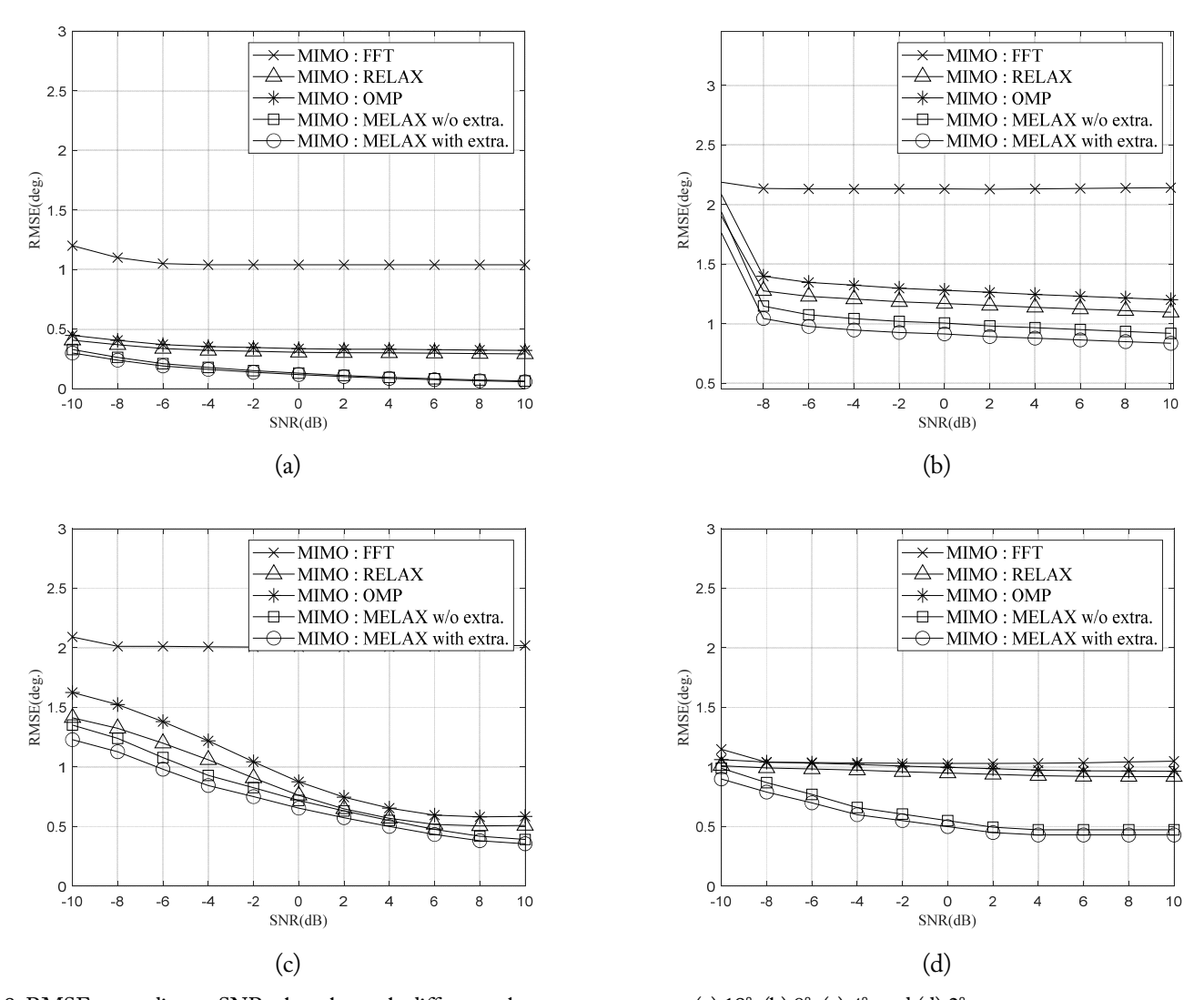


Fig. 8. RMSEs according to SNR when the angle differences between two targets: (a) 18° , (b) 9° , (c) 4° , and (d) 2° .

algorithms have similar accuracy, indicating that all the algorithms are weak at low SNR.

With an angle difference of 4°, the proposed structure in Fig. 8(c) also achieved the best RMSE performance, while the proposed algorithm, OMP, and RELAX algorithm performed similarly because the angle difference is very narrow. With an angle difference of 2°, the proposed structure in Fig. 8(d) performed notably better as regards RMSE than the others. The FFT, OMP, and RELAX algorithms performed similarly but more poorly than the proposed structure. The results in this section demonstrate that the estimation performance of the proposed algorithm with PQ = 12 is better than that of the conventional FFT, OMP, and RELAX with PQ = 12. As indicated in Fig. 6, we configured the FFT size of the range spectrum to 1,024 and showed that the error of the angle estimation approached about 0.5° when the angle difference was 2°.

Next, we examine the RMSEs between the proposed structure and the conventional structures in the presence of a clutter. In the case of certain specified SNR, this simulation obtains the RMSEs of the first target when there are two targets according to the change of the signal-to-clutter ratio (SCR). The Weibull distribution is used for clutter. The probability density function of the Weibull distribution is expressed as:

$$P(x) = \frac{bx^{b-1}}{a^b} \exp\left\{-\left(\frac{x}{a}\right)^2\right\},\tag{16}$$

where x is the random variable, a is the shape parameter, and b is the scale parameter. In automotive radar or drone applications, most stationary clutter is caused by wooden poles, for which the Weibull parameters are set to a=1 and b=1 [17]. This simulation was also performed at angle intervals of 18° , 9° , 4° , and 2° . In Fig. 9(a), since all algorithms are well distinguished at an angle interval of 18° , no significant difference in RMSEs is noted. In Fig. 9(b), at 9° , it can be seen that the proposed structure and RELAX structure achieve better RMSE performances than the FFT. Fig. 9(c) shows similar results to Fig. 9(b), confirming that the proposed and RELAX structures perform better in RMSE than the FFT. Fig 9(d) shows that the proposed algorithm

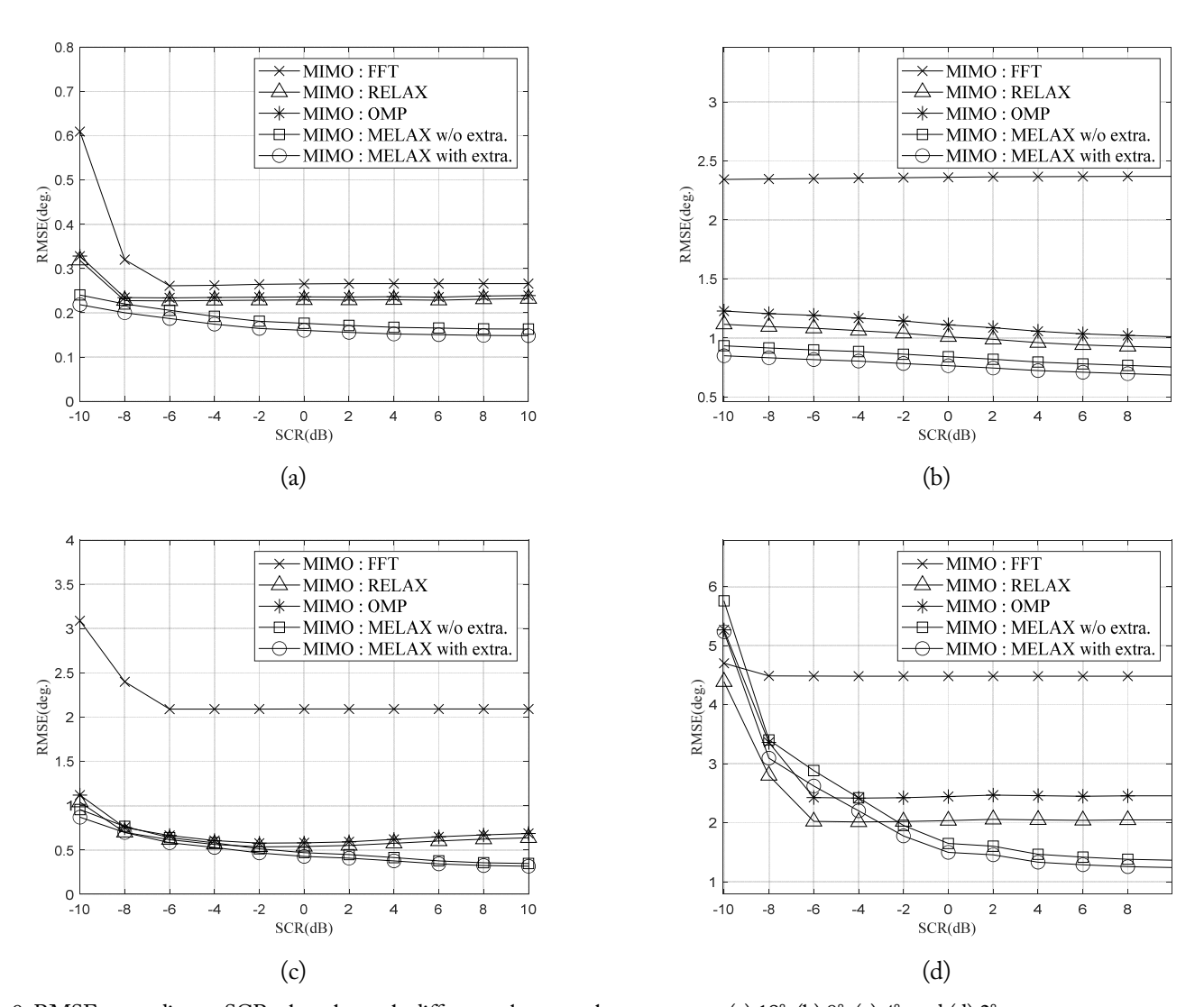


Fig. 9. RMSEs according to SCR when the angle differences between the two targets: (a) 18° , (b) 9° , (c) 4° , and (d) 2° .

achieves better resolution than conventional algorithms at an angle interval of 2°. In Fig. 9(d), the proposed method is based on the MUSIC algorithm, while the conventional RELAX algorithm is based on FFT. According to [18], the MUSIC algorithm, which utilizes singular value decomposition (SVD) or EVD, tends to suffer from performance degradation in low-SNR environments. Therefore, it is understandable that the RMSE performance of the MUSIC-based proposed structure deteriorates compared to the RELAX algorithm under conditions where the SCR is below -4 dB. However, the proposed structure clearly exhibits superior performance when the SCR is above -4 dB.

3. Complexity Analysis

In this chapter, we perform a complexity analysis following the simulation results presented in the previous section. The complexity of the conventional PQ-point FFT in (17) for angle estimation is represented in [11]. In (18), the RELAX algorithm's complexity is M times PQ-point FFT. The OMP algorithm is based on (19) [19]. The proposed algorithm in (20)

consists of LC-MUSIC and extrapolation. The LC-MUSIC algorithm consists of the autocorrelation matrix, EVD, and spectrum generation by region of interest, as shown in (20). The extrapolation uses the prediction order N_p and the number of extrapolated samples K_E . In Fig. 10, the MUSIC algorithm has the highest complexity, while the FFT and extrapolation methods have lower complexity. The proposed structure features a complexity that lies between that of MUSIC and FFT.

$$PQ\log\left(PQ\right),\tag{17}$$

$$MPQ\log(PQ),$$
 (18)

$$\frac{5M}{3} + 2M^2PQ + \frac{M^3}{3} + MPQ,\tag{19}$$

$$PQN_{p} + (K_{E} - PQ)N_{p} + \frac{MLPQ(PQ + 1)}{2} + \frac{16}{5}M(PQ)^{3} + \frac{MPQ(PQ + 1)(PQ - M)}{2} + M^{2}PQ(PQ + 1).$$
(20)

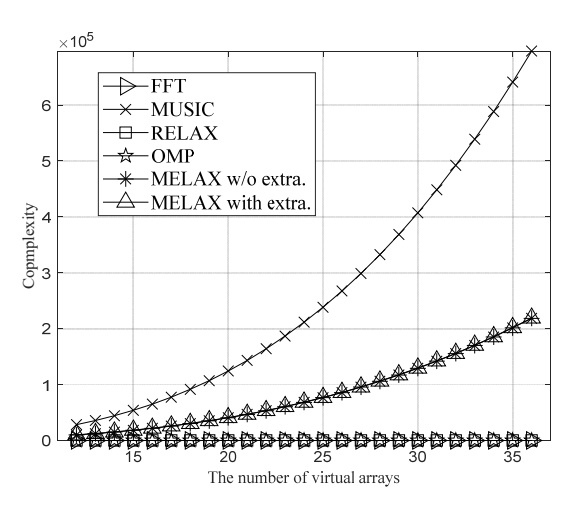


Fig. 10. Complexity analysis.

V. EXPERIMENTS

To assess the estimation performance, this section provides an experimental estimation performance of the proposed and conventional algorithms, including FFT and RELAX, for MIMO FMCW radar. The experiment was conducted in an indoor room. All the experimental parameters are provided.

1. Experimental Explanation

A 77-GHz FMCW radar system, with the parameters listed in Table 1 of [20], was employed for the experiments. The FMCW radar system can synthesize a MIMO radar with PQ=12 virtual receivers, providing high angular resolution. The system consisted of an integrated phase-locked loop (PLL), transmitter, receiver, and ADC. The transmitter included a ramp generator, synthesizer, phase shifter, and power amplifier with a power output of 13 dBm. Each transmitter antenna had an azimuth beamwidth of 72° and an elevation beamwidth of 36° , which was the same as that of the receiver. The receiver included low-noise amplifiers, a mixer, an intermediate frequency filter, and an ADC. The receiver's noise figure was 12 dB, and the phase noise at 1 MHz was -96 dBc/Hz at 76-77 GHz and -94 dBc/Hz at 77-81 GHz.

For the experiments, corner reflectors were used in an indoor room as detailed in Fig. 11. The range estimation was performed using a 1,024-point FFT.

2. Experimental Results

The experimental results verify the performance of the proposed algorithm in estimating the angular parameters of targets compared to conventional algorithms. The study focuses on achieving high-resolution FMCW results by extracting the signal region of the targets and removing clutter in an indoor environment. The experiments were conducted to analyze the range



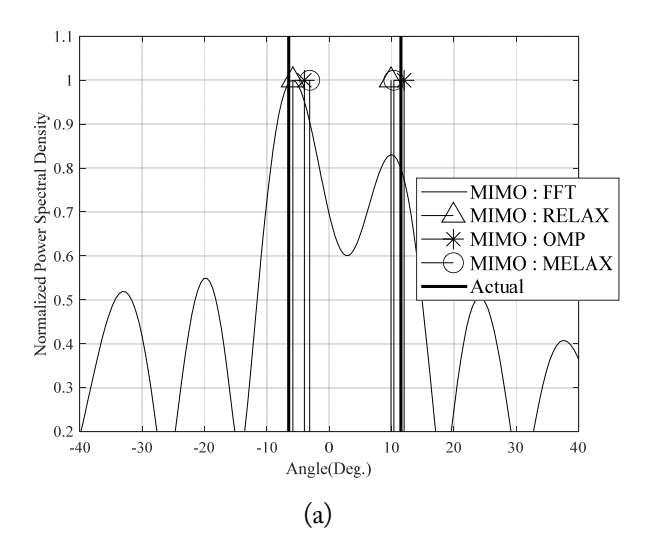
Fig. 11. Experimental environment with two corner reflectors.

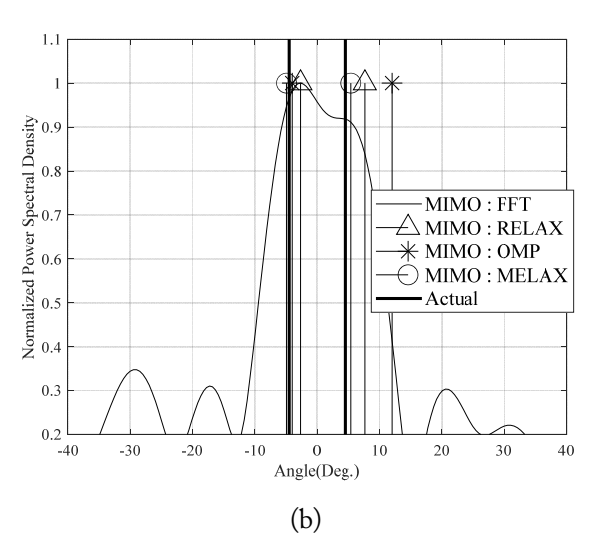
and angular parameters of targets, as presented in Table 2. The estimated positions obtained with the proposed algorithm were compared to the actual positions. Two far-field targets, namely, corner reflectors and humans, were placed at S = 2 m. For cases I, II, and III, two corner reflectors were placed in the indoor room, as shown in Fig. 11. Fig. 12(a) shows that the proposed algorithm and conventional algorithms can separate the two corner reflectors for case I with an angle difference of 18°, which is a wide-angle difference. With an angle difference of 9°, when the angle difference of the two corner reflectors approaches the resolution limit, as shown in Fig. 12(b), the proposed algorithm and RELAX obtained two peaks, while the conventional FFT algorithm failed to separate the targets. In case III, when the two targets were placed very close together at an angle difference of 4°, the proposed algorithm was able to separate the two peaks, while the conventional algorithms obtained only one peak, as shown in Fig. 12(c).

The human-based experimental environments were set up as shown in Fig. 13, with both the corner reflectors and humans located at the same range from the radar. The proposed approach was able to classify two human targets in an indoor room when they were located at a certain range and angle difference, as demonstrated in Fig. 13. The experimental estimation results with humans are presented in Fig. 13. In Fig. 14(a), for case I with a wide angular difference of 1°, both the conventional and proposed structures were able to distinguish between the two humans. As the angle difference reduced to 9°, approaching the resolution limit, Fig. 14(b) shows that the spectrum of the proposed algorithm and RELAX obtained two peaks, while the

Table 2. Summary of the experimental environments

Parameter	Case I	Case II	Case III
Range, S (m)	2	2	2
Angle, θ (°)	18	9	4





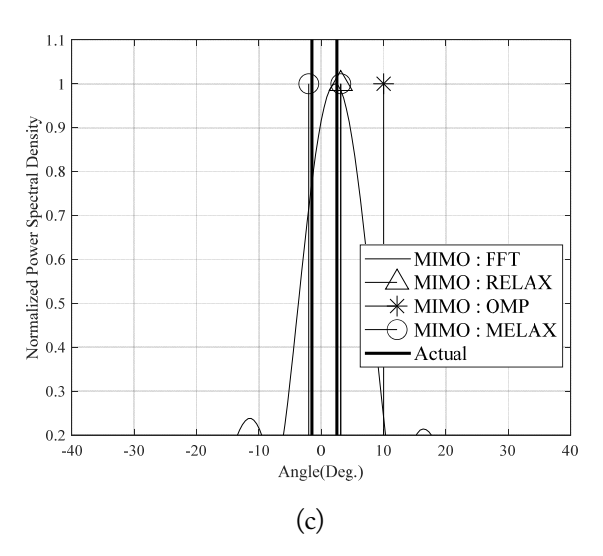


Fig. 12. Experimental spectrum results with angle differences between two corner reflectors of (a) 18°, (b) 9°, and (c) 4°.

conventional FFT algorithm failed to classify the two targets. In case III, where the two targets were placed very close together at an angle difference of 4°, Fig. 14(c) shows that the proposed



Fig. 13. Two-human-based experimental environment.

algorithm was able to distinguish two peaks in the spectrum, while the conventional FFT and RELAX algorithms were unable to separate them.

VI. CONCLUSION

This paper presents a novel super-resolution angle estimation algorithm using LC-MELAX for MIMO FMCW radar. The proposed method significantly enhances angular resolution compared to conventional algorithms, especially when two targets are located very close to each other. Unlike the conventional algorithms that use only one algorithm, the proposed LC-MELAX algorithm uses a combination of RELAX and LC-MUSIC. The simulation results based on a virtual MIMO array of PQ = 12 show that all the algorithms can differentiate between two targets when the angle difference value between them is 18°. However, with an angular separation of 2° between two targets, the proposed algorithm can distinguish them, while the FFT and RELAX-based conventional algorithms cannot. When the angular difference between two targets is set to 18°, both the proposed and conventional schemes maintain consistently low RMSEs across all SNR values. However, when the angular difference value is below the resolution limit at 2°, the proposed algorithm performs better than the conventional FFT and RELAX algorithms. Experimental analyses confirm that the proposed method can identify two targets that cannot be separated by the conventional FFT and RELAX algorithms. Based on its superior performance, the proposed method is highly applicable for FMCW radar.

This work was supported by the DGIST and in part by the DGIST R&D Program of the Ministry of Science, ICT and Future Planning, Korea (No. 25-IT-01 & 25-DPIC-04) and by the Basic Science Research Program through the National Research Foundation of Korea (NRF) funded by the Ministry of Education (No. 2022R1F1A1063386).

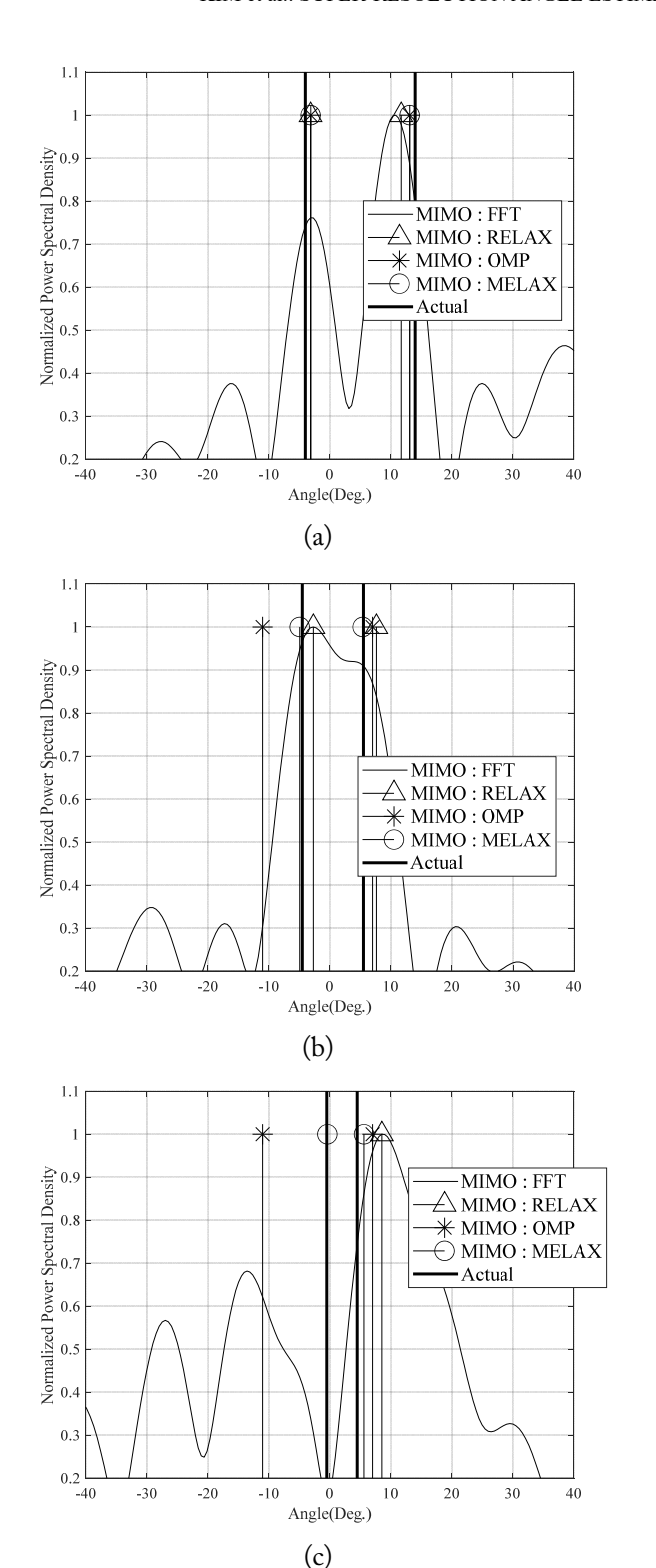


Fig. 14. Experimental spectrum results of angle difference between two humans of (a) 18°, (b) 9°, and (c) 4°.

REFERENCES

[1] X. Fang, J. Li, Z. Zhang, and G. Xiao, "FMCW-MIMO radar-based pedestrian trajectory tracking under low-observable environments," *IEEE Sensors Journal*, vol. 22, no. 20, pp. 19675-

- 19687, 2022. https://doi.org/10.1109/JSEN.2022.3203154
- [2] D. Schwarz, N. Riese, I. Dorsch, and C. Waldschmidt, "System performance of a 79 GHz high-resolution 4D imaging MIMO radar with 1728 virtual channels," *IEEE Journal of Microwaves*, vol. 2, no. 4, pp. 637-647, 2022. https://doi.org/10.1109/JMW.2022.3196454
- [3] B. S. Kim, Y. Jin, J. Lee, and S. Kim, "FMCW radar estimation algorithm with high resolution and low complexity based on reduced search area," *Sensors*, vol. 22, no. 3, article no. 1202, 2022. https://doi.org/10.3390/s22031202
- [4] S. Saponara and B. Neri, "Radar sensor signal acquisition and multidimensional FFT processing for surveillance applications in transport systems," *IEEE Transactions on Instrumentation and Measurement*, vol. 66, no. 4, pp. 604-615, 2017. https://doi.org/10.1109/TIM.2016.2640518
- [5] Y. Dai, T. Jin, H. Li, Y. Song, and J. Hu, "Imaging enhancement via CNN in MIMO virtual array-based radar," *IEEE Transac*tions on Geoscience and Remote Sensing, vol. 59, no. 9, pp. 7449– 7458, 2021. https://doi.org/10.1109/TGRS.2020.3035064
- [6] S. Sun, A. P. Petropulu, and H. V. Poor, "MIMO radar for advanced driver-assistance systems and autonomous driving: advantages and challenges," *IEEE Signal Processing Magazine*, vol. 37, no. 4, pp. 98-117, 2020. https:// doi.org/10.1109/MSP.2020.2978507
- [7] Y. Li, C. Gu, and J. Mao, "4-D gesture sensing using reconfigurable virtual array based on a 60-GHz FMCW MIMO radar sensor," *IEEE Transactions on Microwave Theory and Techniques*, vol. 70, no. 7, pp. 3652-3665, 2022. https://doi.org/10.1109/TMTT.2022.3174075
- [8] K. Han and S. Hong, "High-resolution phased-subarray MIMO radar with grating lobe cancellation technique," *IEEE Transactions on Microwave Theory and Tech*niques, vol. 70, no. 5, pp. 2775-278, 2022. https:// doi.org/10.1109/TMTT.2022.3151633
- [9] G. Yang, C. Li, S. Wu, X. Liu, and G. Fang, "MIMO-SAR 3-D imaging based on range wavenumber decomposing," *IEEE Sensors Journal*, vol. 21, no. 21, pp. 24309-24317, 2021. https://doi.org/10.1109/JSEN.2021.3111173
- [10] S. Kim, J. Kim, C. Chung, and M. H. Ka, "Derivation and validation of three-dimensional microwave imaging using a W-Band MIMO radar," *IEEE Transactions on Geoscience* and Remote Sensing, vol. 60, article no. 2006616, 2022. https://doi.org/10.1109/TGRS.2022.3207013
- [11] B. S. Kim, Y. Jin, J. Lee, and S. Kim, "Low-complexity MUSIC-based direction-of-arrival detection algorithm for frequency-modulated continuous-wave vital radar," *Sensors*, vol. 20, no. 15, article no. 4295, 2020. https://doi.org/10.3390/s20154295
- [12] S. Kim, B. S. Kim, Y. Jin, and J. Lee, "Extrapolation-RELAX estimator based on spectrum partitioning for DOA estima-

- tion of FMCW radar," *IEEE Access*, vol. 7, pp. 98771-98780, 2019. https://doi.org/10.1109/ACCESS.2019.2930102
- [13] B. Li, S. Wang, J. Zhang, X. Cao, and C. Zhao, "Fast randomized-MUSIC for mm-Wave massive MIMO radars," *IEEE Transactions on Vehicular Technology*, vol. 70, no. 2, pp. 1952-1956, 2021. https://doi.org/10.1109/TVT.2021.3051266
- [14] M. Kafal and A. Cozza, "Multifrequency TR-MUSIC processing to locate soft faults in cables subject to noise," *IEEE Transactions on Instrumentation and Measurement*, vol. 69, no. 2, pp. 411-418, 2020. https://doi.org/10.1109/TIM.2019.2896369
- [15] S. Gupta, P. K. Rai, A. Kumar, P. K. Yalavarthy, and L. R. Cenkeramaddi, "Target classification by mmWave FMCW radars using machine learning on range-angle images," *IEEE Sensors Journal*, vol. 21, no. 18, pp. 19993-20001, 2021. https://doi.org/10.1109/JSEN.2021.3092583
- [16] B. Kim, B. Kim, and J. Lee, "A novel DFT-based DOA estimation by a virtual array extension using simple multiplications for FMCW radar," *Sensors*, vol. 18, no. 5, article no. 1560, 2018. https://doi.org/10.3390/s18051560

- [17] R. M. Narayanan and B. R. Snuttjer, "Millimeter wave backscatter measurements in support of collision avoidance applications," *International Journal of Infrared and Millimeter Waves*, vol. 18, pp. 2077-2109, 1997. https://doi.org/10.1007/BF02678252
- [18] S. Lee, Y. J. Yoon, J. E. Lee, H. Sim, and S. C. Kim, "Two-stage DOA estimation method for low SNR signals in automotive radars," *IET Radar, Sonar & Navigation*, vol. 11, no. 11, pp. 1613–1619, 2017. https://doi.org/10.1049/iet-rsn.2017.0221
- [19] S. H. Lee, I. O. Choi, M. S. Kang, and K. T. Kim, "Efficient sparse representation algorithm for accurate DOA estimation of multiple targets with single measurement vector," *Microwave and Optical Technology Letters*, vol. 60, no. 1, pp. 31-37, 2018. https://doi.org/10.1002/mop.30908
- [20] P. Goswami, S. Rao, S. Bharadwaj, and A. Nguyen, "Real-time multi-gesture recognition using 77 GHz FMCW MIMO single chip radar," in *Proceedings of 2019 IEEE International Conference on Consumer Electronics (ICCE)*, Las Vegas, NV, USA, 2019, pp. 1-4. https://doi.org/10.1109/ICCE.2019.8662006

Bong-Seok Kim https://orcid.org/0000-0003-4949-0381



received a B.S. in electronics engineering in 2006 and an M.S. and a Ph.D. in information and communications engineering from Yeungnam University, South Korea, in 2009 and 2014, respectively. From 2014 to 2016, he held a postdoctoral position with the Daegu Gyeongbuk Institute of Science and Technology (DGIST), South Korea. Since 2016, he has been with DGIST as a senior research engineer.

His current interests include multi-functional radar systems and radar signal processing.

Jonghun Lee

https://orcid.org/0000-0002-9991-7083



received a B.S. in electronics engineering and an M.S. and Ph.D. in electrical and electronics and computer science from Sungkyunkwan University, South Korea, in 1996, 1998, and 2002, respectively. From 2002 to 2005, he was with Samsung Electronics Company as a senior research engineer. Since 2005, he has been with the Daegu Gyeongbuk Institute of Science and Technology, South Korea, as a principal

research engineer and full professor. His primary research interests include detection, tracking, and recognition for radar (FMCW and UWB radar), radar-based vehicle sensors, and radar signal processing and sensor fusion. He is an IEEE Senior Member.

Youngseok Jin https://orcid.org/0000-0003-3473-4734



received B.S. and M.S. degrees in communication engineering from Daegu University, South Korea, in 2009 and 2012, respectively. Since 2012, he has been with the Daegu Gyeongbuk Institute of Science and Technology, South Korea, as a researcher. His current interests include radar signal processing and implementation in FPGA/DSP.

Sangdong Kim https://orcid.org/0000-0001-5163-540X



received a B.S. from Hanyang University in 2004, an M.S. from Hanyang University in 2006, and a Ph.D. from Kyungpook National University in 2018, all in electronics engineering. From 2015 to 2016, he was a visiting scholar at the University of Florida. From 2022 to 2023, he was a visiting scholar at Pennsylvania State University. Since 2006, he has been a principal researcher and adjunct associate professor with

the Daegu Gyeongbuk Institute of Science and Technology. His research interests include super-resolution algorithms, automotive radar, and user authentication using vital sign radar. He is an IEEE Senior Member.

Ram M. Narayanan https://orcid.org/0000-0003-3568-2702



received a B.Tech. in electrical engineering from IIT Madras, Chennai, India, in 1976 and a Ph.D. in electrical engineering from the University of Massachusetts, Amherst, MA, USA, in 1988. From 1976 to 1983, he was a research and development engineer with Bharat Electronics Ltd., Ghaziabad, India, where he developed microwave communications equipment. In 1988, he joined the Department of

Electrical Engineering, University of Nebraska–Lincoln, Lincoln, NE, USA, where he served as the Blackman and Lederer Professor. Since 2003, he has been a professor of electrical engineering at The Pennsylvania State University, University Park, PA, USA. He has authored or co-authored 180 journal articles and more than 450 conference publications. His current research interests include sensor information analysis, harmonic and nonlinear radar, noise radar, cognitive radar, medical radar, quantum radar, radar networks, and compressive sensing. Dr. Narayanan was the recipient of the 2017 IEEE Warren White Award for Excellence in Radar Engineering. He is a Fellow of the SPIE and the IETE. He is currently a Member of the IEEE Committee on Ultrawideband Radar Standards Development.